Progress In Electromagnetics Research M, Vol. 52, 9–20, 2016

A Novel Resistance Network Node Potential Measurement Method and Application in Grounding Grids Corrosion Diagnosis

Kai Liu[1, *], Fan Yang[1], Xiaoyu Wang[2], Bing Gao[1], Xiaokuo Kou[3], Manling Dong[3], and Ammad Jadoon[1]

Abstract—In this paper, a novel resistance network node potential measurement technique based on 16-channel cycle method is presented, and a grounding grids corrosion diagnosis measurement system with 16 channels is built from this method. Through this measurement system, 1680 valid potential data and 1560 effective branch voltage data can be collected in one measurement by only 16 risers on the grounding grid. The stability error of the excitation current source is less than 0.15%, and the error of the applicable acquisition data is about 1% according to system data tests. Built on the measurements, an underdetermined sensitivity equation for solving the increasing multiple of branch resistance is put in place to determine the corrosion status of grounding grids. The experimental results show that the plenty of data is necessary when solving the underdetermined equation and also show that the system is under a high stability, high accuracy, and can comply with the requirements of corrosion diagnosis for grounding grids.

1. INTRODUCTION

The main objectives of a grounding system is to guarantee personal safety, equipment protection and power supply continuity. A grounding system comprises all the interconnected grounding facilities in a specific area, but its main elements are the grounding grids [1–5]. Since soil erosion deteriorates the grounding performance of a buried conductor, corrosion diagnosis for grounding grids has become an essential research topic.

The electric circuit theory and electromagnetic field theory are widely used to diagnose the corrosion status of the grounding grids in a power substation [6–9]. The electric circuit theory establishes and solves a diagnosis equation that describes the nonlinear relationship between branch resistance and node voltage based on the Tellegon theory [6, 10, 11]. For large-scale grounding grids, a regional corrosion diagnosis method was proposed by establishing a block model [12, 13]. The electromagnetic field theory proposed by Dawalibi [14] measures the surface electromagnetic field and establishes magnetic field inverse equations to detect the corrosion status of grounding grids [15–17]. A method based on Method of Moment to analyze the breaks of grounding grid by harmonic currents was presented in [18]. It can be used to the condition that the grid is in at least ten-layer soil with a frequency of the injected currents up to 1 MHz; however, it has a limit to large scale of substation grounding grid.

For the actual needs of detection and diagnosis, a testing magnetic field system for grounding grid corrosion diagnosis was designed by using a sine wave excitation current [19]. An automation test system for grounding grid corrosion diagnosis was built by using a digital voltage meter and an intelligential switching device [20]. However, both systems have shortcomings of low precision, small measurement region, and most fatal insufficient amount of data.

Received 25 April 2016, Accepted 18 October 2016, Scheduled 7 November 2016

* Corresponding author: Kai Liu (liukai2015@cqu.edu.cn).

[1] Chongqing University, Chongqing 400044, China. [2] State Grid Zhejiang Electric Power Company Metering Center, Hangzhou, Zhejiang 310008, China. [3] State Grid Henan Electric Power Corporation Research Institute, Zhengzhou, Henan 450052, China.

In power substation, the accessible grounding risers are often limited, but the scale of the grounding grids is always with many nodes and branches shown as Fig. 1 which will cause the equation underdetermined. For example, there will be about 50 nodes and 70 branches in a 110-kV substation in general, but the risers are only about 20. So when a corrosion diagnosis equation is built by using these limited risers, the number of unknowns in the equation will be more than the number of equations that can be set up by those limited risers, namely, the equation must be an underdetermined one. Certainly, with the increase of the level of a power substation, the situation will also be the same.

Thus, in order to make the general corrosion diagnosis algorithm for solving the underdetermined equation and to achieve a better accuracy, enough valid voltage data must be obtained through those limited risers by using some suitable ways. So a method of 16-channel circularly inflow and outflow excitation current to the grounding grid for measuring voltage data is proposed. By this method, much more node potential data and branch voltage data can be obtained when using the same number of risers can maximize the use of limited risers to obtain enough potential data information required.

In this paper, in order to obtain plenty of voltage data, a novel resistance network node potential measurement method based on 16-channel cycles is proposed, and a 16-channel corrosion diagnosis system for grounding grids, which has a high stability, high data accuracy and advantage of plenty of data is also designed. Firstly, the data measurement method will be given in Section 2. Secondly, the key technology of the corrosion diagnosis system and the data test are presented in Section 3. Then, the diagnosis algorithm and network tests are presented in Section 4. Finally, the conclusion is provided.

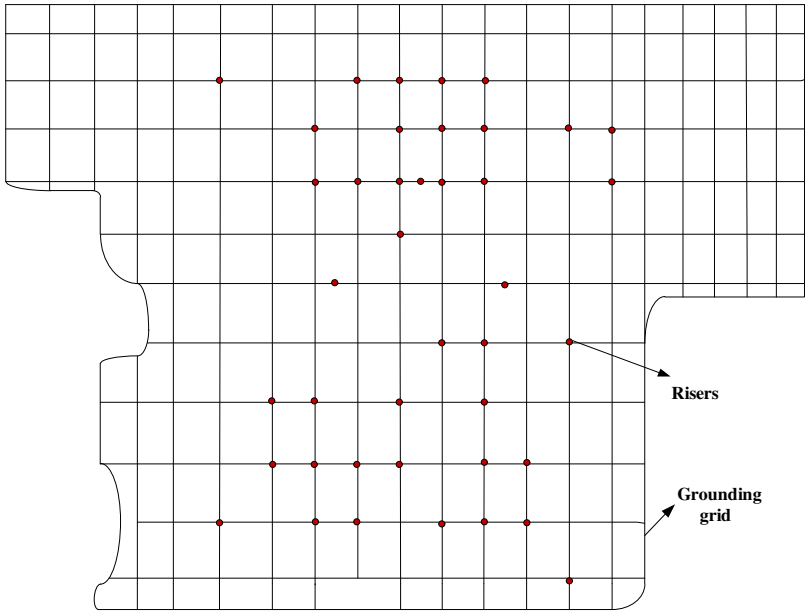

Figure 1. A actual power substation grounding grid model and its part of risers.

2. MEASUREMENT METHODOLOGY

2.1. Principle of Cycle Measurement Method

As shown in Fig. 2, randomly connect 16 substation accessible grounding grid risers with 16 channels of the measurement system, circularly choose two of the nodes as the channel with excitation current inflow and outflow of the grounding grid according to P1-P2, P1-P3, P1-P4, ..., P1-P16; P2-P3, P2-P4, ..., P2-P16; P3-P4, ..., P3-P16; ... P15-P16 (where Px represents node x), and then select the remaining fourteen nodes as the potential measurement nodes. Thus, according to the mathematical combination principle, 120 groups of potential data will be obtained by only sixteen risers through only one measurement.

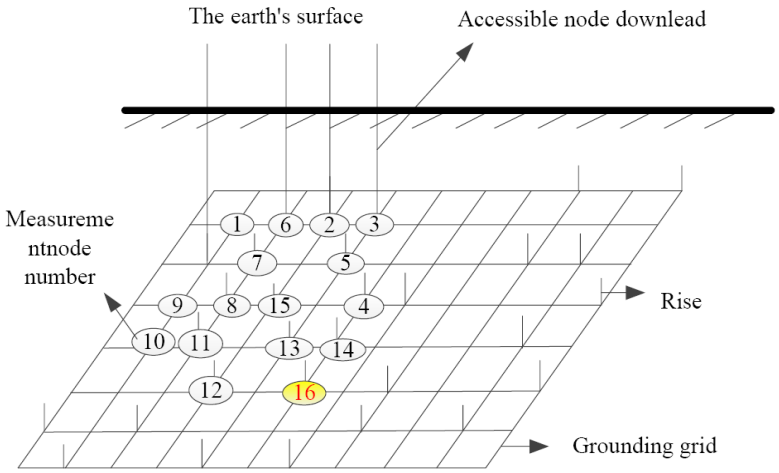

Figure 2. Connected schematic diagram.

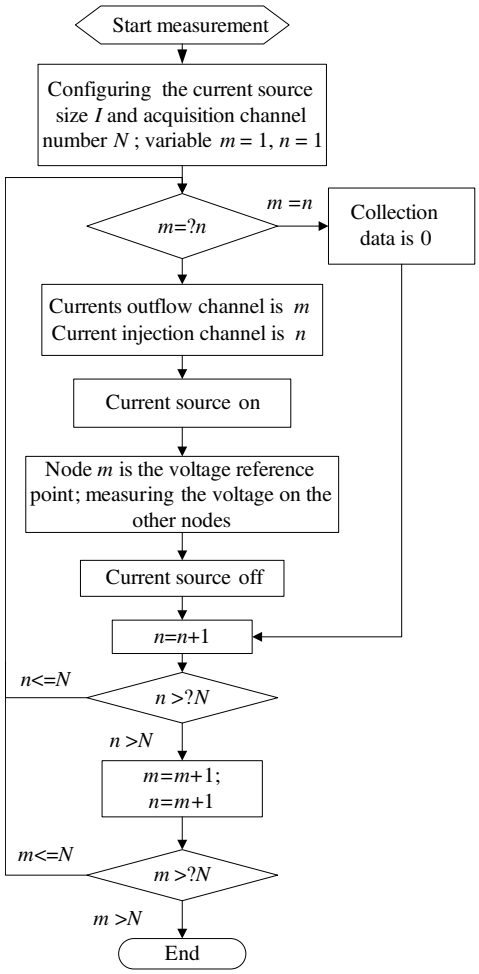

Figure 3. The flow chart of cycle measurement method.

In addition, among each group of potential data, the outflow node is selected as the zero potential reference node, thus there will be 14 effective node potentials in each group of data; so the total number of effective node potential data is $120 \times 14 = 1680$. While to all the potential data, the node whose node number is 16 is chosen as the common zero potential reference node, thus there will be 13 effective branch voltage data in each group of data; that is to say, $120 \times 13 = 1,560$ branch voltage data can be obtained through a single measurement just by using only 16 risers. A flow chart of the cycle measurement method is shown in Fig. 3.

As shown in Fig. 3 above, when starting measurement, we firstly configure the output of the current source I, the number of acquisition channel N and the initial variable $m = 1$ and $n = 1$. Secondly, we judge if m is equal to n or not; if yes, the collection data will be zero and n will self-increase one to $n + 1$; if not, we will make m as the current outflow channel and n as the current injection channel. Thirdly, open the current source, and the node m will be chosen as the voltage reference point and the other nodes as the voltage measuring point. When finishing one voltage acquisition, close the current source and make the n self-increase one to $n+1$. Fourthly, we will judge if n is larger than N or not; if yes, we will make m self-increase to $m + 1$, and n becomes $m + 1$; if not, we will return to the second step. When n is larger than N, after finishing the variable assignments, we will judge if m is larger than N; if yes, the procedure will be over; if not, it will also return to the second step. While m is larger than N, the voltage cycle measurement procedure is over.

In general, the number of acquisition channels, N, will be set to sixteen. However, for those small grounding grids and the number of risers fewer than sixteen, four to sixteen acquisition channels can

also be selected. For those large grounding grids and the number of risers much more than sixteen, a regional measurement method [12, 13] can be chosen.

2.2. Potential Measurement for Single Node

A brief sketch of excitation current circularly inflow and outflow mode is shown in Fig. 4, namely respectively choose node one to node sixteen as the excitation current outflow node, and then successively and circularly increase the excitation current injection node, thus the current exciting way for the grounding grid will be changed, and the responding potential of the same node will be different.

Note node 1 for outflow point and node 2 for injection point as the first current exciting way, node 1 for outflow point and node 3 for injection point as the second current exciting way, node 1 for outflow point and node 4 for injection point as the third current exciting way, ..., node 2 for outflow point and node 3 for injection point as the sixteenth current exciting way node 2 for outflow point and node 4 for injection point as the seventeenth current exciting way ..., and so on, thus there will be a total of 120 groups of current injection and outflow mode (current exciting way). Note each group of responding node potential corresponding to its current exciting way as U_i^j (i = 1, 2, 3, ..., 119, 120; j = 1, 2, 3, ..., 15, 16), where i means the kind of current exciting mode, and j represents the node number. U^j represents the responding digital voltage signal of the excitation current obtained from grounding grid nodes by the A/D chip, U_{ref} the reference voltage of the A/D chip, U_i^{jn} the system measurement potential namely the single node potential shown in Fig. 11, and U_i^{jb} the branch voltage relative to the node 16 as the common zero potential reference node.

Thus, the calculation of the potential of a single node is shown as Formula (1).

$$U_i^{jn} = \frac{u_{ref}}{2^{24}} \times U^j \tag{1}$$

The calculation of the branch voltage relative to the node 16 as the common zero potential reference node is shown as Formula (2).

$$U_i^{jb} = U_i^{jn} - U_i^{16} \tag{2}$$

The potential measurement principle of a single node is shown in Fig. 5. Firstly, the responding node voltages of the excitation current are submitted to the monolithic iCMOS analog multiplexers ADG1206 which comprises sixteen channels and can switch one of the sixteen inputs to a common output, as determined by the 4-bit binary address lines A0, A1, A2, and A3; secondly, the common output is sent to 24 bits A/D data acquisition chip ADS1241 after low-pass filtering [21], thus the analog potential of the single node is converted to a digital potential signal; finally, the digital potential will be sent to the ARM for storage and display.

Because a 24 bits A/D data acquisition chip is used in the measurement system device, the accuracy of the measurement device can reach a level of mV, which enables it to meet the measurement requirement of the small resistance network as substation grounding grids when injecting little excitation current. The measuring range of the system device is 2.5 V.

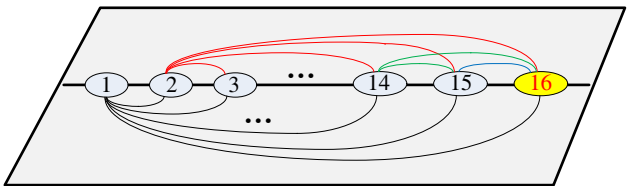

Figure 4. Sketch of excitation current cycle inflow and outflow mode.

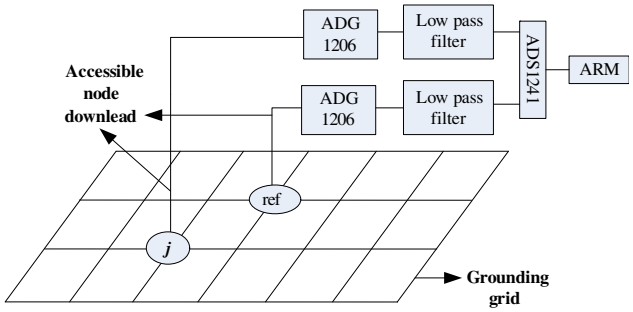

Figure 5. Schematic diagram of potential measurement for single node.

3. MEASUREMENT SYSTEM SETUP AND TESTS

3.1. Excitation Current Source Module

An excitation current source with a feedback structure can produce an adjustable dc current from 0 A to 1 A (Fig. 6).

Voltage signals generated from the 12-bit D/A converter of an Advanced RISC Machine (ARM) microcontroller are processed by a low-pass filter, a subtraction circuit and a positive feedback circuit, and then it is indirectly loaded to a precise resistance for producing the dc current. The output current will be detected by the current detection module before its injection to ensure its accuracy and the ARM microcontroller dynamically adjusts the D/A converter to stabilize the output current, which can ensure the output current error less than 0.15%. When the resistance load is 1 Ω, its output current test curve is shown in Fig. 7.

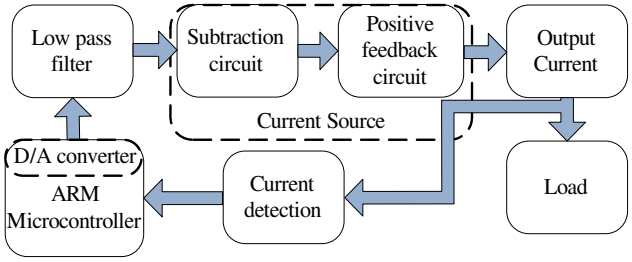

Figure 6. Structure of the excitation current source module.

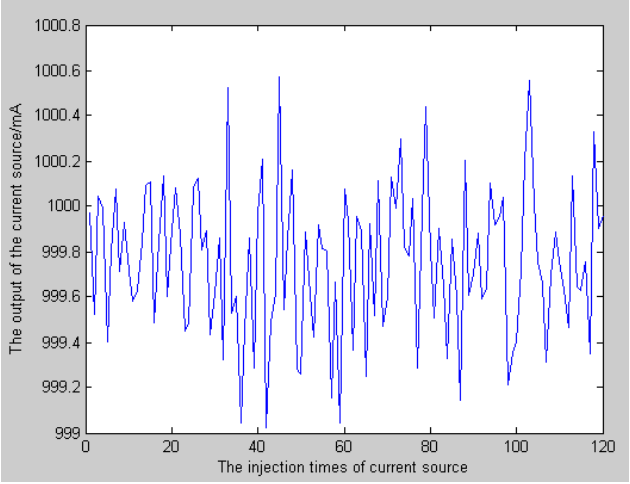

Figure 7. The fixed resistance load test curve.

Furthermore, in order to test the resistance load capacity of the excitation current source, the resistance load was changed to 0.05 Ω, 0.1 Ω, 0.5 Ω, 1.0 Ω, 5.0 Ω, 10.0 Ω, 20.0 Ω, 30.0 Ω and 40.0 Ω, and then its size of output current was measured separately. The corresponding value is shown in Table 1. The resistance load capacity testing diagram is shown in Fig. 8.

The relationship between the output current and the load resistance is shown in Fig. 9. From the test curve shown above we know that when the value of resistance load is smaller than 20.0 Ω, the size of output current is 1.00 A, and when the value of resistance load is bigger than 20.0 Ω, the size of output current will be a little lower than 1.00 A. Thus we can get the conclusion that the current source will also have a high stability when being connected to different loads.

Table 1. The output current result of the different load test.

The value of load/Ω	0.05	0.1	0.5	1.0	5.0	10.0	20.0	30.0	40.0
The size of output current/A	1.00	1.00	1.00	1.00	1.00	1.00	1.00	0.99	0.99

3.2. Current Switching Module

The current switching module consists of multi-channel analog switches, triodes and relays, and it is used to adjust the node's location of current injection and outflow. This module has a symmetrical

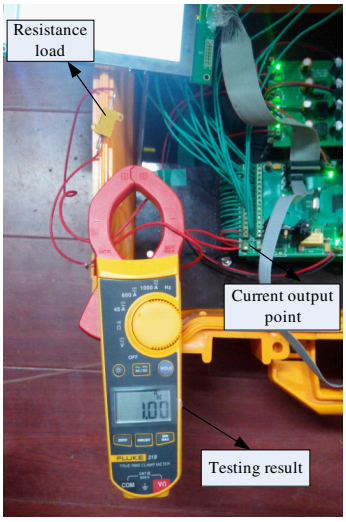

Figure 8. Resistance load capacity testing diagram.

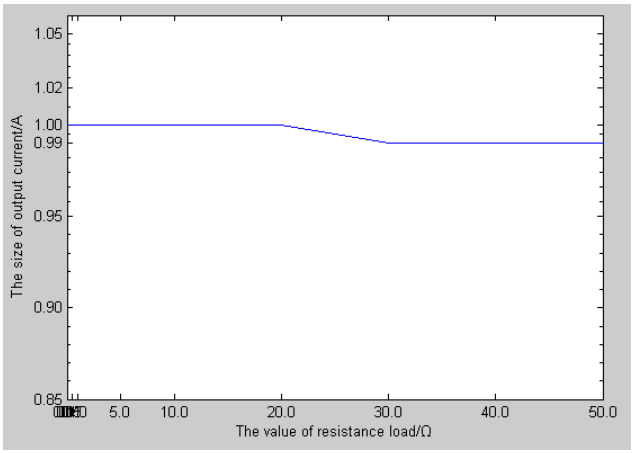

Figure 9. The different resistance load test curve.

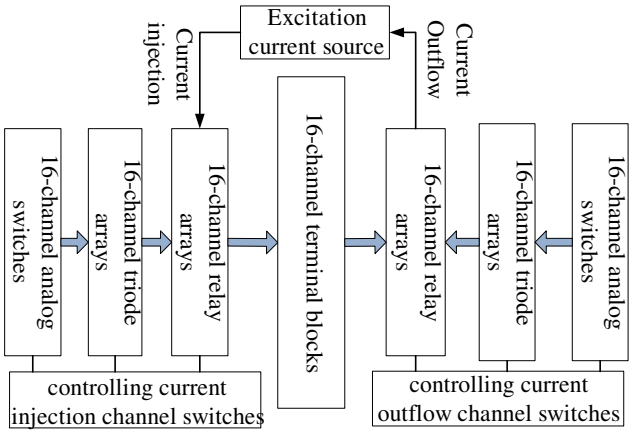

Figure 10. Structure of the current switching module.

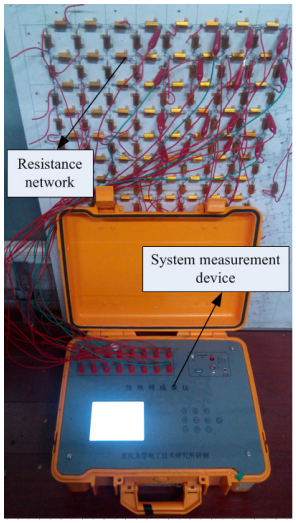

Figure 11. Resistance network measurement schematic diagram.

structure (Fig. 10). The analog switches, triode arrays, relay arrays and terminal blocks all with 16 channels are connected in turn and controlled by the microcontroller.

3.3. Data Test and Error Analysis

After the device was completed, the data were collected by using the resistance network built in the laboratory, whose resistance value was 1 Ω. The measurement schematic diagram is shown in Fig. 11.

As shown above, the 16 channels of this device were separately connected with the 16 node outgoing-lines of the resistance network, which were equivalent to the risers in grounding grids. Two of the channels were chosen as the current injection and outflow node, and the current outflow node was chosen as the zero potential reference node. Thus the measurement voltage data could be obtained which was shown in Fig. 12.

As shown in Fig. 12, the potential of each node was obtained when the current outflow channel was channel one, and the current injection channel was channel two. Getting rid of the potential of current

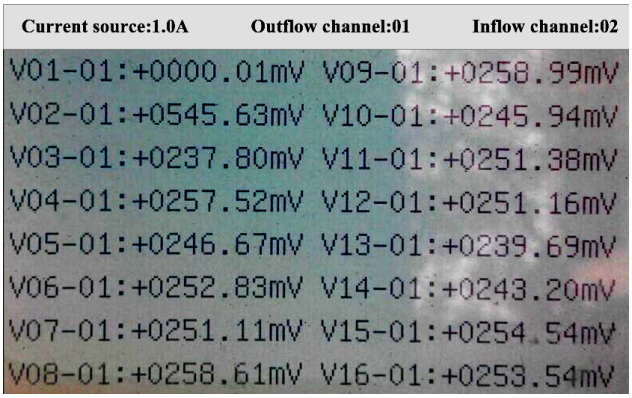

Figure 12. The display of measured node potential data.

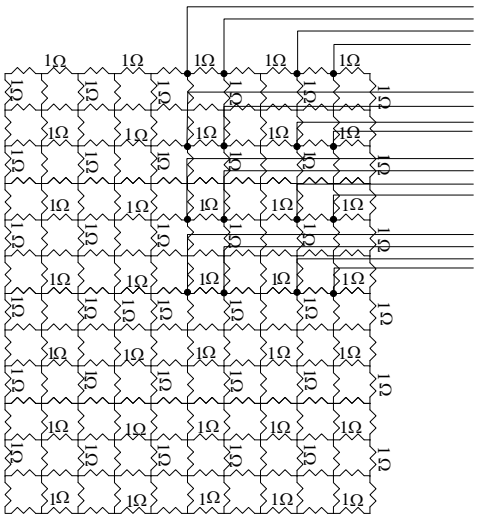

Figure 13. The simulation resistance network by Simulink.

injection and outflow nodes, the remaining fourteen potential data could be used as the valid data, which can support the diagnosis algorithm. From the Fig. 12, we know that fourteen valid potential data could be obtained through one current exciting way. Thus in general, a total of $120 \times 14 = 1,680$ effective potential data could be obtained in only one measurement.

Meanwhile, in order to verify the accuracy of the measured data, a simulation resistance network was built by the Simulink of MATLAB function, which was the same as the laboratory resistance network. The built simulation resistance network is shown in Fig. 13.

In the simulation, two nodes of this resistance network were chosen as the current injection and outflow point. Thus a group of simulation potential data of each node could be obtained by using the same measurement method. Then the accuracy analysis of the device could be completed by comparing with the measured potential data obtained from the measurement device. Part of the comparison results are shown in Table 2.

It is clear from Table 2 that the error of measurement data and simulation data is about 1%, which can meet the minimum permissible error of general algorithm requirement for its data error. Hence it can be concluded from above that the data collected by this method have a relatively high accuracy.

Table 2. Part of the comparison results of the measured data and theoretical data.

Device measured data/mV	Computer simulation data/mV	Measurement error /mV	The percentage error
237.80	237.76	0.04	0.0168%
257.52	254.32	3.20	1.26%
246.67	245.10	1.57	0.641%
252.83	252.20	0.63	0.250%
251.11	250.13	0.98	0.392%
258.61	257.92	0.69	0.268%
258.99	256.23	2.66	1.04%
245.94	245.13	0.81	0.330%
251.38	250.63	0.75	0.300%
251.16	251.06	0.10	0.040%
...	...	...	...

4. APPLICATION

4.1. Diagnosis Algorithm

A reliable diagnosis algorithm will quickly and accurately diagnose the fault branch and its fault status of the network, while the measurement data are transmitted to the PC.

It is assumed that the numbers of nodes and branches in the grounding grids are $N+1$ and B, respectively. The association matrix for this gird is $\mathbf{A}$; the admittance matrix of a branch is $\mathbf{Y}_b$; the nodal admittance matrix is $\mathbf{Y}_n$; $\mathbf{Y}_n = \mathbf{A}\mathbf{Y}_b\mathbf{A}_T$.

$$\mathbf{Y}_b = \begin{bmatrix} R_1^{-1} & 0 & \cdots & 0 \\ 0 & R_2^{-1} & \cdots & 0 \\ \vdots & \vdots & \ddots & \vdots \\ 0 & 0 & \cdots & R_n^{-1} \end{bmatrix} \tag{3}$$

Two nodes of grounding grids are selected, and the excitation current is injected. At time i, the vector of excitation current is $\mathbf{I}_S^i$, and $\mathbf{Y}_n\mathbf{U}_n^i = \mathbf{I}_S^i$. Thus, the total differential of nodal voltage $\mathbf{U}_n^i$ is

$$d\mathbf{U}_n^i = \sum_{k=1}^{B} \frac{\partial(\mathbf{Y}_n^{-1}\mathbf{I}_S^i)}{\partial R_k} dR_k = \sum_{k=1}^{B} \left[\frac{\partial(\mathbf{Y}_n^{-1})}{\partial R_k}\mathbf{I}_S^i + \mathbf{Y}_n^{-1}\frac{\partial(\mathbf{I}_S^i)}{\partial R_k} \right] dR_k \tag{4}$$

Since $\mathbf{I}_S^i$ is constant, its differential is zero.

$$d\mathbf{U}_n^i = \sum_{k=1}^{B} \frac{\partial(\mathbf{Y}_n^{-1}\mathbf{I}_S^i)}{\partial R_k} dR_k = \sum_{k=1}^{B} \frac{\partial(\mathbf{Y}_n^{-1})}{\partial R_k}\mathbf{I}_S^i dR_k \tag{5}$$

Thus $d\mathbf{U}_n^i = \mathbf{P}^i d\mathbf{R}$, where $\mathbf{P}^i$ is an $N \times B$ matrix and only relates to the pattern of current excitation and the shape of grounding grids. $\mathbf{P}^i$ reflects the effect of branch resistance variation on the node voltage and is called a sensitivity matrix.

For data measurement of grounding grids at time T, a sensitivity equation is established:

$$\begin{bmatrix} d\mathbf{U}_n^1 \\ d\mathbf{U}_n^2 \\ \vdots \\ d\mathbf{U}_n^T \end{bmatrix} = \begin{bmatrix} \mathbf{P}^1 \\ \mathbf{P}^2 \\ \vdots \\ \mathbf{P}^T \end{bmatrix} d\mathbf{R} \tag{6}$$

That

$$d\mathbf{U}_n = \mathbf{P}d\mathbf{R} \tag{7}$$

Thus solving this problem is converted into solving a least squares problem:

$$\min \ \|\mathbf{P}d\mathbf{R} - d\mathbf{U}_n\|_2 \tag{8}$$

Formula (6) is an underdetermined equation, which needs enough voltage data to obtain a solution that is close to the real value [22, 23]. The least squares orthogonal decomposition (LSQR) regularization algorithm was used to solve the problem, and for each branch, we calculated its resistance $d\mathbf{R}$ and detected its corrosion and breakage status. If the increasing multiple of branch resistance is larger, the corrosion of grid branch will be more serious.

In order to test the accuracy and stability of the measurement system, a laboratory test was first conducted, and then the substation grounding grid tests were done.

4.2. Laboratory Test

A 5×5 resistance network equivalent to a grounding grid was built (Fig. 14), and the branch resistance was $1\,\Omega$. The 16-channel measurement device was connected with the sixteen nodes of the grounding grid model (Fig. 15). When starting the measurement, the channel 16 was chosen as the zero potential reference node.

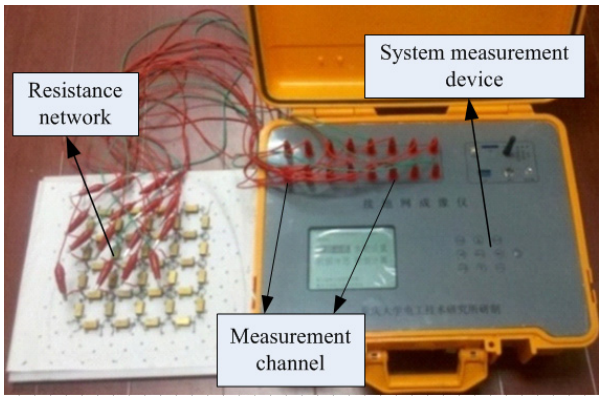

Figure 14. Experimental grid and the connection diagram.

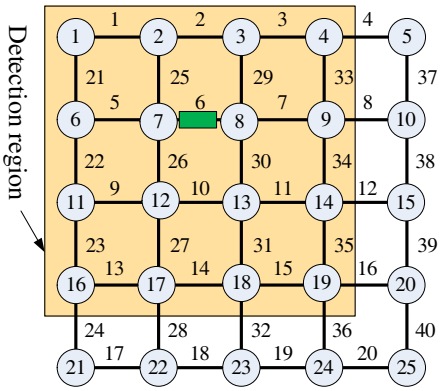

Figure 15. Topology of the grid model.

In this test, branch 6 was disconnected to simulate a branch broken fault. The device was used to obtain the potential data, with an injection excitation current of 1.0 A.

Diagnostic algorithm was used to analyze the measured potential data. A single group of measured data and multiple groups of measured data obtained by the device were respectively used for the calculation of broken branch detection. The results are shown in Fig. 16 and Fig. 17.

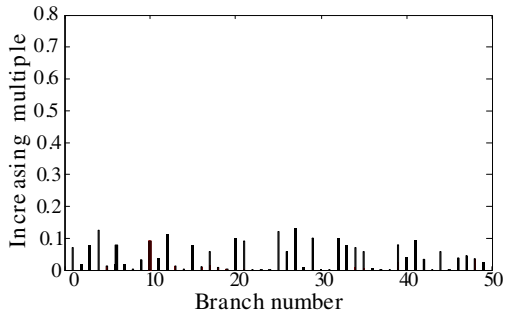

Figure 16. Diagnosis result by using a single group of data.

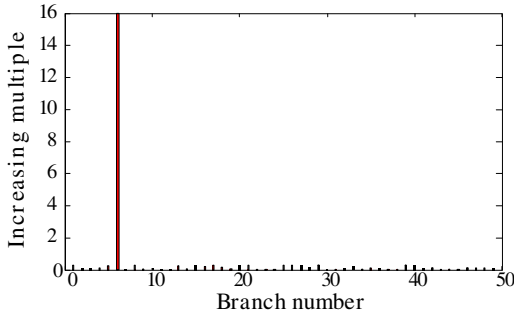

Figure 17. Diagnosis result by using multiple groups of data.

From Fig. 16, we know that all the branches have a very small increasing multiple, namely a good status according to the calculation result, which is not corresponding with the actual situation of the network because of the insufficient amount of data. However, from Fig. 17 it can be seen that the increasing multiple of branch 6 is very large, and the others are very small, which indicate that branch 6 had serious corrosion fault according to the calculation result. That is to say, the calculation result matched with the actual situation due to the use of multiple groups of measurement data.

Seen from the comparison of the calculation results obtained by using different numbers of data, it is known that the plenty of data was very significant for the diagnosis algorithm to solve an underdetermined equation, and the device can provide plenty of data. In addition, the laboratory resistance network test validated the effectiveness of the diagnostic algorithm and the reliability of the measurement system, and also enabled the system to be applied to the practical corrosion diagnosis of grounding grids.

4.3. C Substation Grounding Grid Test

An abandoned 110 kV substation which had run for 25 years was selected for the substation grounding grid test (Fig. 18). Since the substation was large, the grounding grid was divided into several diagnosis

Figure 18. Connection diagram for field test.

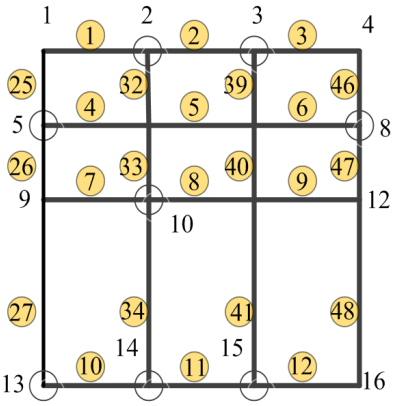

Figure 19. Topology of region 1.

Figure 20. Disconnect branch.

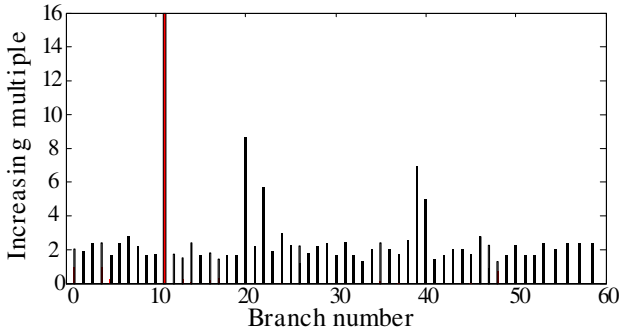

Figure 21. Diagnosis result of field test by using multiple groups of data.

regions. Diagnostic results could accurately reflect the grounding grid corrosion status of each region. The topology of region 1 as an example is shown in Fig. 19.

The original status of branch 11 was normal. The depth of the grounding grid branch was 1.6 m. In order to make the diagnosis result more obvious, branch 11 was artificially broken (Fig. 20). The diagnosis algorithm was used to calculate the result (Fig. 21) on MATLAB, and multiple groups of data were also used. From the diagnosis result, we know three messages.

I, The resistance value of all grounding grid branches in this substation had an increase of two times or much more than the initial value.

II, Branch 11 had an increasing multiple of 16, which was much larger than other branches.

III, The branches near branch 20 and branch 40 had a increase of roughly eight times.

According to the actual situation of this selected substation, the steels used for the grounding grid should be corroded after buried in the soil and bearing the leakage current for so many years. Thus we can consider that message I is marched with this situation. Branch 11 had been artificially broken, so message II was also marched with the actual situation. In addition, branch 20 and branch 40 are both the connection location with the neutral grounding point of the main transformer, which will lead to a faster corrosion of the steels, so they will have a much more increasing multiple than other branches. That is to say, message III is also marched with the actual situation.

Generally speaking, we can think that the diagnosis result is matched with the actual situation. Thus the substation grounding grid test also validated that the measurement system could be used for corrosion fault diagnosis of grounding grids.

5. CONCLUSION

A novel resistance network node potential measurement method based on 16-channel cycle technique is proposed, and a 16-channel corrosion diagnosis system based on this method is built for grounding grids. The system has the following features: 1) plenty of measurement data provided by 16-channel cycle measurement method; 2) high stability in the excitation current source; 3) high accuracy in data acquisition; 4) large fault diagnosis region; 5) reliable diagnosis algorithm. Measurement data fully reflect the impedance status of grounding grids in the measurement area. The sensitivity equation based on the data can accurately locate the corrosion branch. Tests results show that the accuracy and stability of the measurement system meet the requirements of corrosion diagnosis for grounding grid.

ACKNOWLEDGMENT

This work was supported by the National Natural Science Foundation of China (Grant No. 51477013), 2014 Chongqing University Postgraduates' Innovation Project, Project Number: CYS14012.

REFERENCES

1. Dimopoulos, A., H. Griffiths, N. Harid, et al., "Proposal for probabilistic risk assessment in grounding systems and its application to transmission substations," *IEEE Trans. Power Del.*, Vol. 27, No. 4, 2219–2226, Oct. 2012.
2. *IEEE Guide for Safety in AC Substation Grounding*, IEEE Std 80-2000, 2000.
3. Long, X., M. Dong, W. Xu, et al., "Online monitoring of substation grounding grid conditions using touch and step voltage sensors," *IEEE Transactions on Smart Grid*, Vol. 3, No. 2, 761–769, Jun. 2012.
4. Sverak, J. G., W. Wang, Y. Gervais, X. D. Do, and D. Mukedkar, "A probabilistic method for the design of power grounding systems," *IEEE Trans. Power Del.*, Vol. 7, No. 3, 1196–1206, Jul. 1992.
5. Sverak, J. G., W. K. Dick, T. H. Dodds, and R. H. Heppe, "Safe substation grounding-part I," *IEEE Transactions on Power Apparatus and Systems*, Vol. 100, 4281–4290, Sep. 1981.
6. Celli, G., E. Ghiani, and F. Pilo, "Behaviour of grounding systems: A quasi-static EMTP model and its validation," *Electric Power Systems Research*, Vol. 85, 24–29, Apr. 2012.
7. Heimbach, M. and L. D. Grcev, "Grounding system analysis in transients programs applying electromagnetic field approach," *IEEE Trans. Power Del.*, Vol. 12, No. 1, 186–193, Jan. 1997.
8. Dommel, H. W., "Digital computer solution of electromagnetic transient in single and multiple networks," *IEEE Trans. Power App. Syst.*, Vol. 88, No. 4, 388–399, Apr. 1969.
9. Otero, A. F., J. Cidras, and J. L. del Alamo, "Frequency-dependent grounding system calculation by means of a conventional nodal analysis technique," *IEEE Trans. Power Del.*, Vol. 14, No. 3, 873–878, Jul. 1999.
10. Lawson, V. R., "Problems and detection of line anchor and substation ground grid corrosion," *IEEE Transactions on Industry Applications*, Vol. 24, No. 1, 25–32. Jan.–Feb. 1988,
11. Patel, S., "A complete field analysis of substation ground grid by applying continuous low voltage fault," *IEEE Trans. Power App. Syst.*, Vol. 104, No. 8, 2238–2243, Aug. 1985.
12. Liu, J., Y. Ni, S. Wang, et al., "Grounding grids corrosion diagnosis using a block dividing approach," *High Voltage Engineering*, Vol. 37, 1194–1202, May 2011 (in Chinese).
13. Ni, Y. F., J. Liu, S. Q. Wang, et al., "Splitting method for grounding grids corrosion diagnosis using a block dividing approach," *High Voltage Engineering*, Vol. 37, 2250–2260, Sep. 2011 (in Chinese).
14. Dawalibi, F., "Electromagnetic fields generated by overhead and buried short conductors part 2 — ground networks," *IEEE Trans. Power Delivery*, Vol. 1, 112–119, Oct. 1986.
15. Yan, M., G. G. Karady, and S. Kucuksari, "Testing continuity of grounding grid using the AC current injection method," *IEEE Power and Energy Society General Meeting*, 1–6, 2010.

16. He, W., Q. Shi, F. Yang, et al., "Computation method of magnetic field inverse problem on grounding grids fault diagnosis," *Journal of Chongqing University*, Vol. 35, 80–85, Sep. 2012 (in Chinese).
17. Huang, L. and D. G. Kasten, "Modeling of ground grid and metallic structure currents in high voltage a.c. substations for the computation of electromagnetic fields," *Electric Power Systems Research*, Vol. 59, 31–37, Mar. 2001.
18. Zhang, B., Z. Zhao, X. Cui, et al., "Diagnosis of breaks in substation's grounding grid by using the electromagnetic method," *IEEE Trans. Magn.*, Vol. 38, 473–476, Mar. 2002.
19. Liu, Y., X. Cui, and Z. Zhao, "Design and application of exciting power for substation grounding grids tests system based on impedance transformation technology," *Proceedings of the CSEE*, Vol. 28, 18–23, Oct. 2008 (in Chinese)
20. Cheng, H., Y. Yang, J. Liu, et al., "Grounding grids corrosion diagnosis automation test system and its key techniques," *High Voltage Engineering*, Vol. 35, 2989–2994, Dec. 2009 (in Chinese).
21. Texas Instruments Inc. ADS1241E datasheet, [Online], Available: http://www.ti.com/product/ads1241.
22. Kubica, B. J., "Interval methods for solving underdetermined nonlinear equations systems," *Reliable Computing*, Vol. 15, No. 3, 207–217, Jul. 2011.
23. Zeng, J., S. Lin, and Z. Xu, "Sparse solution of underdetermined linear equations via adaptively iterative thresholding," *Signal Processing*, Vol. 97, 152–161, Apr. 2014.